A Fuzzy Gain-scheduler for the Attitude Control of an Unmanned Helicopter

Bourhane Kadmiry, *Member, IEEE,* and Dimiter Driankov, *Member, IEEE*

***Abstract*— In this paper we address the design of an attitude controller that achieves stable, and robust aggressive maneuverability for an unmanned helicopter. The controller proposed is in the form of a fuzzy gain-scheduler, and is used for stable and robust altitude, roll, pitch, and yaw control. The controller is obtained from a realistic nonlinear MIMO model of a real unmanned helicopter platform, the APID-MK3. The results of this work are illustrated by extensive simulation, showing that the objective of aggressive, and robust maneuverability has been achieved.**

***Index Terms*— unmanned helicopter, Takagi-Sugeno fuzzy control, fuzzy gain scheduling, output-feedback fuzzy control.**

I. INTRODUCTION

THE work reported in this paper is a contribution to the overall objective of the *Wallenberg Laboratory for Information Technology and Autonomous Systems* (WITAS): the development of an intelligent, deliberative/reactive command and control system, containing active-vision sensors, which supports the operation of a unmanned air vehicle (UAV) in both semi- and full-autonomy modes. The particular problem addressed here is the design of an altitude and attitude (roll, pitch, and yaw) controller that achieves *stable and robust aggressive maneuverability for an unmanned helicopter*. We define aggressive maneuverability –in the sense of attitude control– as i) controlling in the whole range of the attitude angles of the UAV, and ii) tracking a given trajectory at the highest possible velocity.

If aggressive maneuverability in these terms is achieved, the controller described here executes, in a stable and robust manner: i) *tracking of trajectories describing curvilinear translational (or horizontal) motion at relatively high speed and constant altitude*, and ii) *set-point regulation for fast translational acceleration/deceleration, hovering, and climb*. The robustness of the flight controller is defined as its ability to compensate for: i) *external disturbances in terms of wind gusts*, ii) *model parameter uncertainties in terms of changing payload*, and iii) *sensor noise for attitude control signals*.

The flight controller presented here is obtained and tested in simulation using a realistic nonlinear MIMO model of a real unmanned helicopter platform, the APID-MK3. We are completely aware that the ”realism” of the results reported in this work w.r.t the above aims is limited by the fact that *all the work is performed in simulation*. However, since the mathematical model used for simulation is close enough –from control point of view– to the real APID-MK3 system we have all reasons to believe in the realism of these results.

The paper is organized as follows. Section II describes related work on aggressive maneuverability for unmanned helicopters. Section III presents the control scheme for the attitude controller and defines the control tasks to be executed by it. Section IV introduces fuzzy gain-scheduled control (FGS). Section V presents the design of the attitude controller: It takes desired attitude angles and altitude as inputs, and generates the actuator deflections that will result in that attitude and altitude. Section VI presents the result of simulations showing that the objective of aggressive, and robust maneuverability has been achieved. In Section VII we provide the reader with some conclusions.

II. RELATED WORK ON AGGRESSIVE MANEUVERABILITY

In recent years, the design and implementation of control algorithms for unmanned helicopters has been the object of quite a number of studies, see [2]–[8], [10], [15]. Of all those, there are only two studies reported aimed at achieving aggressive maneuverability. In [2], aggressive maneuverability is defined as *the ability to track fast trajectories*, which is very much in line with our understanding of this notion. In [2], this ability is realized by controlling over the full overall operational flight envelope, while in our case, it is realized by expanding the control to the use of the full range of the rotor attitude angles. This in turn implies that we also are able to achieve the practically available capabilities within the flight envelope. However neither in [2] nor in any other related publication (see [4]) are there any results (in simulation or on the real platform) reported, from which one can ”quantify” the aggressive maneuverability the authors have in mind.

In [3], aggressive maneuverability is translated into a *minimum time optimal control problem* within the constraints of the helicopter’s capabilities over the flight envelope. Only simulation results illustrating this approach are reported. However, the word aggressive in [3] has a broader meaning: the authors are not interested in executing an aggressive maneuver for its own sake (e.g. flying at high speed along a given trajectory), but –because the aggressive maneuver will place the helicopter in a more favorable position– to reach a predetermined given goal (e.g. moving to a certain location evading a threat). In contrast to that, we are just interested in being able to perform aggressive maneuvers, and not to appropriately select and initiate such maneuvers from a predefined maneuvers set.

In the case of APID-MK3, the need for aggressive maneuverability –for its own sake– comes from the fact that

Manuscript received January 20, 2004; revised March 31, 2004.
This work was supported by the Alice & Knut Wallenberg Foundation
B. Kadmiry is with the Linköping University, Sweden.
D. Driankov is with the Örebro University, Sweden

the current control system existing on the helicopter platform does not utilize large ranges of the rotor attitude angles. This produces lower rate-of-change of the body attitude angles. Consequently, the control is done on rather small ranges and restricts the magnitude of the curvature of the trajectory which these angles can follow at a given relatively high speed. Furthermore, control within small ranges for the body attitude angles implies small acceleration rate – a shortcoming when a ground object is capable of accelerating at higher rates. Last but not least, the ability to decelerate fast is necessary for safe navigation. That is for instance, when possible obstacles (e.g. electrical lines,...) have to be avoided as fast as possible. In this context, our objective will be the design of an attitude controller which acts on much larger ranges of the body attitude angles, i.e., $\phi \in [-\pi/4, +\pi/4]$, $\theta \in [-\pi/4, +\pi/4]$, and $\psi \in [-\pi, +\pi]$, by utilizing the full range of the rotor attitude angles. The latter are approximated to the interval $[-0.25, +0.25]$ rad, which translates to the main rotor cyclic's. In addition to that, the controller should also achieve robust and stable tracking of trajectories with varying curvature magnitude at relatively high speed.

III. The control scheme

VTOL vehicles of any kind are maneuvered by controlling their attitude angles, i.e., roll, pitch, and yaw. Fig. 1 presents the control loop for the altitude/attitude controller. It takes desired attitude angles $(\phi, \theta, \psi)^d$ for a given desired altitude z^d and outputs cyclic angles (ϕ_c, θ_c), and collective angles (θ_M, θ_T) to control the main and tail rotors respectively. One

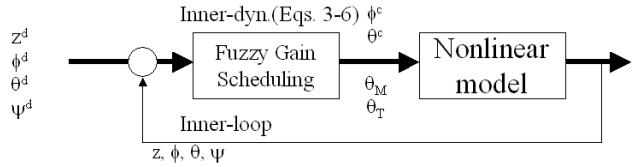

Fig. 1. Control scheme for the attitude/altitude controller

important reason for having altitude/attitude controller is as follows. The vertical motion of the helicopter depends on the relation between its weight and the lift force generated by the main rotor blades. If the lift force is greater than the weight, the helicopter accelerates upwards (climb); if it is less than the weight, the helicopter accelerates downwards (descent); and if it is equal to the weight, the helicopter remains at a constant altitude (hover). The horizontal motion of the helicopter (longitudinal – along the x-axis; and lateral – along the y-axis) occurs when there is a horizontal force component. Such a force is generated by inclining the lift force in the desired direction, inducing by that the thrust force. However, because of the coupling between the different types of motion, the following effect is observed: when the lift force is inclined, creating a horizontal motion (thrust/drag), the magnitude of the vertical component is decreased under the action of the weight, thus, causing a loss of altitude. That is why we would like to control the attitude angles in such a way so that a desired horizontal motion is produced, but without loss of altitude. This obviously can be achieved by a controller that is able to simultaneously regulate both the attitude angles and the altitude.

IV. Fuzzy gain scheduling for dynamic output-feedback control

The attitude and altitude dynamics of a helicopter are a typical example of a nonlinear MIMO plant. However, there is no general method for designing nonlinear controllers. What is available today, is a collection of alternative and complementary techniques, each of them been best applicable within a particular class of nonlinear systems. This explains why the helicopter's original nonlinear model has to be "modified" –in one way or another– so that a particular design technique to be used. In this context, the advantage of using Takagi-Sugeno (TS) models is that a large class of nonlinear plants[1], including the attitude dynamics of a helicopter, can be well represented by these models, without the need to modify the original nonlinear dynamics in any significant way. The particular TS-model used in our work to represent the helicopter's altitude/attitude dynamics is of the general form

$$\begin{aligned} \dot{x} &= \sum_{i=1}^{l} w_i(\theta)(A_i x + B_i u + a_i) \\ y &= \sum_{i=1}^{l} w_i(\theta)(C_i x + c_i) \end{aligned} \tag{1}$$

where $A_i \in R^{n\times n}$, $B_i \in R^{n\times m}$, $a_i \in R^n$, $C_i \in R^{p\times n}$, and $c_i \in R^p$. The model described in (1) is obtained from the original nonlinear altitude/attitude model by using a method called sector-bounded non-linearities (see [12] and [13]). For details, the reader is referred to [16], and an example is given in Section V-A.

A. T-S dynamic output-feedback controllers

We will concentrate here on output-feedback controllers and we will constrain the model with certain assumptions when necessary. It it is also assumed that the varying parameters in θ are measurable. Consider the system given in (1)

$$\begin{aligned} \dot{x} &= A(\theta)x + B(\theta)u + a(\theta) \\ y &= C(\theta)x + c(\theta) \end{aligned} \tag{2}$$

where $A(\theta) = \sum_{i=1}^{l} w_i(\theta)(A_i)$,$B(\theta) = \sum_{i=1}^{l} w_i(\theta)(B_i)$, and $C(\theta) = \sum_{i=1}^{l} w_i(\theta)(C_i)$. Equation (2) can be thought of as a polytopic linear parameter varying (LPV) system subjected to certain disturbances, stemming from the affine terms. The idea here is to make use of the framework for gain scheduled $\mathcal{H}_\infty$ controllers in order to: i) Shape the closed loop transient dynamics so that it conforms to the performance specifications, and ii) Design the controller to reject the influence of the affine terms. We will concentrate on the first step for the moment. In [9] it is shown how to design a gain scheduled controller with guaranteed $\mathcal{H}_\infty$ performance

γ for the following general LPV system

$$\begin{aligned} \dot{x} &= A(\theta)x + B_1(\theta)w + B_2(\theta)u \\ z &= C_1(\theta)x + D_{11}(\theta)w + D_{12}(\theta)u \\ y &= C_2(\theta)x + D_{21}(\theta)w + D_{22}(\theta)u \end{aligned} \tag{3}$$

where $A \in R^{n\times n}$, $B_1 \in R^{n\times m_1}$, $B_2 \in R^{n\times m_2}$, $C_1 \in R^{p_1\times n}$, and $C_2 \in R^{p_2\times n}$. θ is allowed to vary in a parameter box Θ with (l) extreme points and the LPV matrices depend affinelly on θ. Equation (3) is therefore constrained to vary in a polytope with vertices given by the extreme points in Θ. Thus, setting $a(\theta) = 0$, and $c(\theta) = 0$ in (2) yields to a system that can be written in the form of (3). In addition, the following assumptions must hold:

Assumption 1: $D_{22}(\theta) = 0$ or D_{22i} = 0 for $i = 1, \ldots, l$.

Assumption 2: $B_2(\theta)$, $C_2(\theta)$, $D_{12}(\theta)$, and $D_{21}(\theta)$ are parameter independent or $B_{2i} = B_2$, $C_{2i} = C_2$, $D_{12i} = D_{12}$, and $D_{21i} = D_{21}$ for $i = 1, \ldots, l$.

Assumptions (1) and (2) may seem to be restrictive in practice. However, it is often possible to augment the plant with linear filters representing the actuator and sensor dynamics and thereby make the input and output matrices parameter independent. The objective is to find an internally stabilizing parameter-dependent dynamic output feedback controller, with the infinity norm of the transfer function from w to z less than γ, $\|T_{zw}\|_\infty \leq \gamma$, of the form

$$\begin{aligned} \dot{x}_c &= A_K(\theta)x_c + B_K(\theta)y \\ u &= C_K(\theta)x_c + D_K(\theta)y \end{aligned} \tag{4}$$

with the controller parameters

$$\Omega(\theta) := \begin{bmatrix} A_K(\theta) & B_K(\theta) \\ C_K(\theta) & D_K(\theta) \end{bmatrix} \in \text{Co}\left\{ \begin{bmatrix} A_{Ki} & B_{Ki} \\ C_{Ki} & D_{Ki} \end{bmatrix} \right\}, \quad for \quad i = 1, \ldots, l \tag{5}$$

From the convex solvability condition theorem [9], there exists a LPV controller that guarantees quadratic $\mathcal{H}_\infty$ performance γ over Θ if and only if there exist symmetric matrices R, $S \in \mathcal{R}^{n\times n}$ satisfying the $2r + 1$ linear matrix inequalities

$$\begin{aligned} \tilde{\mathcal{N}}_R^T \left[\begin{array}{cc|c} A_iR + RA_i^T & RC_{1i}^T & B_{1i} \\ C_{1i}R & -\gamma I & D_{11i} \\ \hline B_{1i}^T & D_{11i}^T & -\gamma I \end{array}\right] \tilde{\mathcal{N}}_R &< 0, \\ \tilde{\mathcal{N}}_S^T \left[\begin{array}{cc|c} A_i^TS + SA_i & SB_{1i} & C_{1i}^T \\ B_{1i}^TS & -\gamma I & D_{11i}^T \\ \hline C_{1i} & D_{11i} & -\gamma I \end{array}\right] \tilde{\mathcal{N}}_S &< 0, \\ for i = 1, \ldots, l \quad , and \quad \left[\begin{array}{cc} R & I \\ I & S \end{array}\right] &\geq 0 \end{aligned} \tag{6}$$

with

$$\tilde{\mathcal{N}}_R = \left[\begin{array}{c|c} \mathcal{N}_R & 0 \\ \hline 0 & I \end{array}\right] \quad \text{and} \quad \tilde{\mathcal{N}}_S = \left[\begin{array}{c|c} \mathcal{N}_S & 0 \\ \hline 0 & I \end{array}\right],$$

where $\mathcal{N}_R$ and $\mathcal{N}_S$ denote the null space of (B_2^T, D_{12}^T) and (C_2, D_{21}) respectively. If a feasible solution is found, a closed loop Lyapunov matrix X_{cl} can be obtained by computing (via singular value decomposition) two matrices M and N such that

$$MN^T = I - RS \tag{7}$$

and solve the following matrix equation for X_{cl}

$$\begin{bmatrix} S & I \\ N^T & 0 \end{bmatrix} = X_{cl} \begin{bmatrix} I & R \\ 0 & M^T \end{bmatrix} \tag{8}$$

Now, given a closed loop Lyapunov matrix X_{cl} the vertice controllers

$$\Omega_i = \begin{bmatrix} A_{Ki} & B_{Ki} \\ C_{Ki} & D_{Ki} \end{bmatrix} \tag{9}$$

can be found (from the use of the bounded real lemma, see e.g. [14], extended to polytopic systems) by solving the following system of LMIs

$$\begin{bmatrix} A_{cli}^TX_{cl} + X_{cl}A_{cli} & X_{cl}B_{cli} & C_{cli}^T \\ B_{cli}^TX_{cl} & -\gamma I & D_{cli}^T \\ C_{cli} & D_{cli} & -\gamma I \end{bmatrix} < 0$$

with $i = 1, \ldots, l$,, and

$$\begin{aligned} A_{cli} &= \begin{bmatrix} A_i + B_2D_{Ki}C_2 & B_2C_{Ki} \\ B_{Ki}C_2 & A_{Ki} \end{bmatrix}, \\ B_{cli} &= \begin{bmatrix} B_{1i} + B_2D_{Ki}D_{21} \\ B_{Ki}D_{21} \end{bmatrix} \\ C_{cli} &= \begin{bmatrix} C_{1i} + D_{12}D_{Ki}C_2 & D_{12}C_{Ki} \end{bmatrix}, \\ D_{cli} &= \begin{bmatrix} D_{11i} + D_{12}D_{Ki}D_{12} \end{bmatrix} \end{aligned}$$

Thus, a LPV controller can be designed for the linear part of (2). The controller is then parameterized n-line by using measurements of θ, and the convex decomposition given by the fuzzy rule base, i.e., the convex combination:

$$\begin{bmatrix} A_K(\theta) & B_K(\theta) \\ C_K(\theta) & D_K(\theta) \end{bmatrix} = \sum_{i=1}^{l} w_i(\theta) \begin{bmatrix} A_{Ki} & B_{Ki} \\ C_{Ki} & D_{Ki} \end{bmatrix} \tag{10}$$

Due to assumptions (1) and (2), the affine term $c(\theta)$ disappears, and attention must only be given to $a(\theta)$. The approach taken here is to consider $a(\theta)$ as a "measurable" disturbance. That is, given a particular θ from measurements, it is always possible to compute the disturbance $a(\theta)$ acting on the model. By feed-forward of the computed $a(\theta)$ to the controller it is possible to make the controller compensate for it, see Fig. 2. Modelling the disturbance and its measurement is easily done by adding entries in B_1 and D_{21} respectively. The controller is then synthesized according to the steps outlined above.

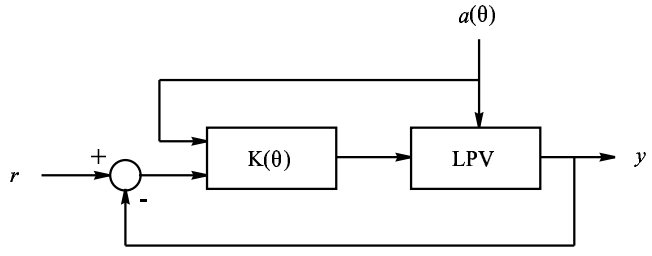

Fig. 2. Closed loop with an affine term as a "measurable" disturbance

V. The Design of a Fuzzy Attitude/Altitude Controller

The current control system for APID-MK3 does not utilize the full range of the rotor attitude angles. As a consequence, this produces lower rate-of-change of the attitude angles ϕ, θ, and ψ, and consequently the control is done on rather small ranges for these – all this prevents aggressive maneuverability. In order to achieve the latter, the objective of our study is to design an attitude controller which acts on much larger ranges of the attitude angles, i.e., $-\pi/4 \leq \phi \leq +\pi/4, -\pi/4 \leq \theta \leq +\pi/4, -\pi \leq \psi \leq +\pi$, by utilizing the full range of the rotor attitude angles. The latter, for the purpose of this study, are in the interval $[-0.25, 0.25]$ rad.

The design approach used here consists of the following steps:

- Decoupling the nonlinearities in the control inputs by adding first-order actuator transfer functions – as a result, the nonlinearities are moved into the state;
- The new model is linearized by bounding the nonlinearities in the state by linear functions – in this way the nonlinear model is approximated by a TS-fuzzy model, which boils down to convex combination of linear sub-models;
- A gain scheduled output feedback $\mathcal{H}_\infty$ controller for the so-obtained approximated model is designed.

In what follows we will describe in more detail the above three steps of the design. The original mathematical model used for the attitude/altitude control of APID-MK3, defined in the inertial frame, is of the form:

$$\begin{aligned} \ddot{z} &= \frac{1}{m}(Z_w + Z_s - K_M\Omega_M^2\theta_M \cos\phi\cos\theta) \\ \ddot{\phi} &= -a\dot{\phi} + dK_M\Omega_M^2(b_{1s} + N_\phi)\theta_M \\ \ddot{\theta} &= -b\dot{\theta} - eK_M\Omega_M^2(a_{1s} + N_\theta)\theta_M \\ \ddot{\psi} &= -c\dot{\psi} + f((\theta_T + N_\psi) + \psi_T) \end{aligned} \tag{11}$$

where the state vector is $(z, \phi, \theta, \psi, \dot{z}, \dot{\phi}, \dot{\theta}, \dot{\psi})$, i.e., altitude, attitude angles, and their respective rates. The control inputs are $(b_{1s}, a_{1s}, \theta_M, \theta_T)$, i.e., these are the usual control inputs in terms of lateral and longitudinal cyclic's, and collective angles for the main and tail rotors. The first equation describes the dynamics of altitude motion where Z_w is a wind force in the z-axis, and Z_s is the gravity force on the cabin. $(N_\phi, N_\theta, N_\psi)^T$ represents the sensor-noise associated with the attitude angles. $a, b, c, d, e, f, K_M, \Omega_M$, and ψ_T are model parameters. The above model has to be transformed in the form of (2), with the vector $a(\theta)$ being the affine term representing wind accelerations and attitude angles noise $a(\theta) = (\frac{Z_w}{m}, N_\phi, N_\theta, N_\psi)^T$. All the outputs of the model are directly measurable (attitude angles and their rates, position, and velocity). Thus the expression in (2) is reduced to the identity matrix and $c(\theta) = 0$. In the model described in (11), the control inputs are produced by servo-actuators. Thus, we will complete (11) by introduce the transfer functions that relate the outputs from these servo-actuators to the control inputs. The servo-actuators used in APID-MK3 are first-order transfer functions with saturation, augmented with a linear model for the Bell-Hiller mixer, and angles-to-signals plus

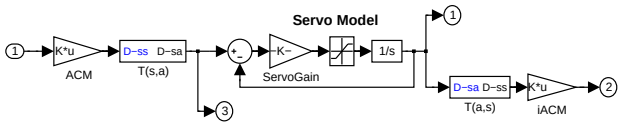

Fig. 3. Servo-actuators with Bell-Hiller mixer diagram

signals-to-angles transformations, as illustrated in teh block-diagram in Fig. 3. The servo-actuator model will be simplified

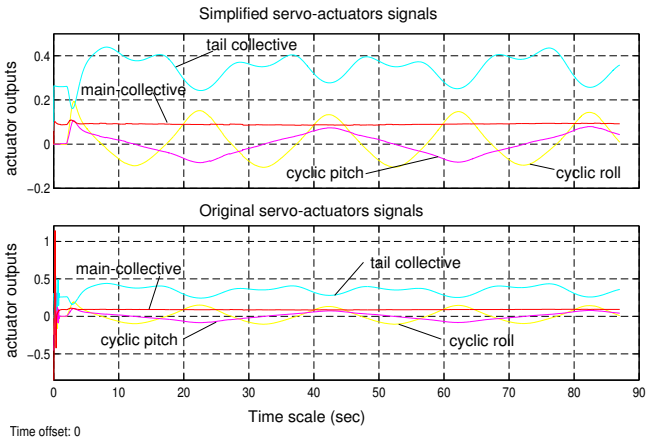

Fig. 4. Servo-actuators boundaries for the simplified (up), and the original (down)

in the form of a first-order function which still obeys the constraints for the actuated signals to be within the range [-1.8, +1.8] for (b_{1s}, a_{1s}), and [-1, +1] for (θ_M, θ_T). We verify that the outputs produced from the original, (see Fig. 4 bottom-part), and simplified servo-actuators, (see Fig. 4 upper-part) –once proportionally amplified– are very similar, and are still within the range [-1, +1]. This in turn implies that the rotor angles produced by the servo-actuators' outputs are realistic, that is they are within their admissible ranges (approx. [-0.25, +0.25] rad). The simplified expression for the servo-actuators transfer functions are as follows

$$\begin{aligned} \dot{b}_{1s} &= -300\, b_{1s} + 300\, u_{b_{1s}}, \\ \dot{a}_{1s} &= -300\, a_{1s} + 300\, u_{a_{1s}}, \\ \dot{\theta}_M &= -300\, \theta_M + 300\, u_{\theta_M}, \\ \dot{\theta}_T &= -300\, \theta_T + 300\, u_{\theta_T}, \end{aligned} \tag{12}$$

Now, we can expand the model with the above actuators whose outputs are the cyclic angles (b_{1s}, a_{1s}), and the collective angles (θ_M, θ_T), and whose inputs are the signals $(u_{b_{1s}}, u_{a_{1s}}, u_{\theta_M}, u_{\theta_T})$. As a result, this will shift the nonlinearities –due to couplings between the control inputs– into nonlinearities between the state variables, as mentioned in Section IV-A. As a result, the model in (11) becomes as

follows:

$$\begin{aligned}
\dot{x}_3 &= x_9 \\
\dot{x}_4 &= x_{10} \\
\dot{x}_5 &= x_{11} \\
\dot{x}_6 &= x_{12} \\
\dot{x}_9 &= \frac{1}{m}(Z_w + Z_s - K_M\Omega_M^2 x_{15}(\cos x_{10}\cos x_{11})) \\
\dot{x}_{10} &= -a\, x_{10} + dK_M\Omega_M^2\, x_{15}(x_{13} + N_\phi) \\
\dot{x}_{11} &= -b\, x_{11} - eK_M\Omega_M^2\, x_{15}(x_{14} + N_\theta) \\
\dot{x}_{12} &= -c\, x_{12} + f\,((x_{16} + N_\psi) + \psi_T), \\
\dot{x}_{13} &= -300\, x_{13} + 300\, u_{b_{1s}}, \\
\dot{x}_{14} &= -300\, x_{14} + 300\, u_{a_{1s}}, \\
\dot{x}_{15} &= -300\, x_{15} + 300\, u_{\theta_M}, \\
\dot{x}_{16} &= -300\, x_{16} + 300\, u_{\theta_T}
\end{aligned} \tag{13}$$

where the $(x_3, ...x_6, x_9, ...x_{12})$ corresponds to $(z, \phi, \theta, \psi, \dot{z}, \dot{\phi}, \dot{\theta}, \dot{\psi})$, i.e., altitude, attitude angles, and their respective rates. $(x_{13}, ..., x_{16})$ are $(b_{1s}, a_{1s}, \theta_M, \theta_T)$, i.e., these are the usual control inputs in terms of lateral and longitudinal cyclic's, and collective angles for the main and tail rotors. Furthermore, $u_{b_{1s}}$, $u_{a_{1s}}$, u_{θ_M}, and u_{θ_T} are the commanded cyclic roll and pitch together with the main and tail rotor collective angles. Notice that b_{1s}, a_{1s}, θ_M, and θ_T are now pseudo state variables.

A. Linearization of the attitude/altitude model

Consider again the model described in (13). For each of the nonlinear terms in this model we choose a linear bounding such that the fuzzy system obtained represents exactly the nonlinear system. Now, we consider $\cos(x_{10})\cos(x_{11})x_{15}$, $x_{13}x_{15}$, and $x_{14}x_{15}$ to be the nonlinear terms subject to linear bounding – these reside in the altitude, roll and pitch equations associated respectively with $\dot{x}_9$, $\dot{x}_{10}$, and $\dot{x}_{11}$ respectively. The state variables involved in these nonlinear terms satisfy:

$$x_{10}, x_{11} \in [-\pi/4,\ \pi/4], \quad \text{and} \quad x_{15} \in [\pi/18,\ 5\pi/18] \tag{14}$$

The state variable x_{15} is trivially bounded by

$$0.1745 < x_{15} < 0.8727. \tag{15}$$

$\cos(x_{10})$ and $\cos(x_{11})$, taking into account the bounds from (14), can be bounded by the two constant functions:

$$0.7071 < \cos(x_{10}) < 1\ , \quad 0.7071 < \cos(x_{11}) < 1. \tag{16}$$

The above bounds result in

$$0.5 < \cos(x_{10})\cos(x_{11}) < 1. \tag{17}$$

Then the above three nonlinear terms can be represented via the use of the derived upper and lower bounds in the following manner:

$$\begin{aligned}
x_{13}x_{15} &= F_1^1 0.8727 x_{13} + F_1^2 0.1745 x_{13}, \\
x_{14}x_{15} &= F_1^1 0.8727 x_{14} + F_1^2 0.1745 x_{14}, \\
\cos(x_{10})\cos(x_{11})x_{15} &= F_2^1 x_{15} + F_2^2 0.5 x_{15},
\end{aligned}$$

where $F_1^1,\ F_2^1 \in [0, 1]$, $F_1^2 = 1 - F_1^1$, and $F_2^2 = 1 - F_2^1$. By solving the above equations for F_1^1, F_1^2, F_2^1, and F_2^2 we obtain the following membership functions:

$$\begin{aligned}
F_1^1(x_{15}) &= (x_{15} - 0.1745)/0.6981, \\
F_1^2(x_{15}) &= (0.8727 - x_{15})/0.6981, \\
F_2^1(x_{10}, x_{11}) &= 2\cos(x_{10})\cos(x_{11}) - 1, \\
F_2^2(x_{10}, x_{11}) &= 2 - 2\cos(x_{10})\cos(x_{11}).
\end{aligned}$$

The graphs of the membership functions F_1^1 and F_1^2 related to the roll and pitch angles are shown in Fig. 5 left-side, and the graphs of F_2^1 and F_2^2 related to the collective pitch are shown in Fig. 5 right-side.

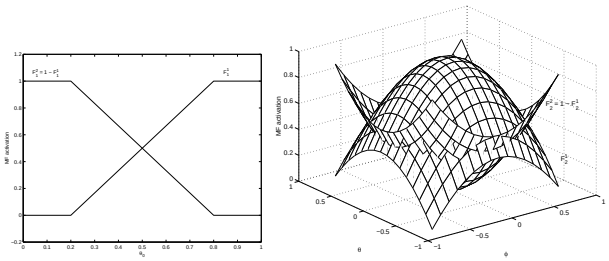

Fig. 5. Membership functions $F_1^{(.)}$ and $F_2^{(.)}$

1) Controller design: The fuzzy model, with respect to (1) is then expressed as the following set of only four rules:

$$\begin{aligned}
1 \ &: \ \text{IF } x_{15} \text{ is } F_1^1 \text{ and } \cos(x_{10})\cos(x_{11}) \text{ is } F_2^1 \\
&\quad \text{THEN} \quad \dot{x} = A_1 x + Bu + a(\theta), \\
2 \ &: \ \text{IF } x_{15} \text{ is } F_1^1 \text{ and } \cos(x_{10})\cos(x_{11}) \text{ is } F_2^2 \\
&\quad \text{THEN} \quad \dot{x} = A_2 x + Bu + a(\theta), \\
3 \ &: \ \text{IF } x_{15} \text{ is } F_1^2 \text{ and } \cos(x_{10})\cos(x_{11}) \text{ is } F_2^1 \\
&\quad \text{THEN} \quad \dot{x} = A_3 x + Bu + a(\theta), \\
4 \ &: \ \text{IF } x_{15} \text{ is } F_1^2 \text{ and } \cos(x_{10})\cos(x_{11}) \text{ is } F_2^2 \\
&\quad \text{THEN} \quad \dot{x} = A_4 x + Bu + a(\theta).
\end{aligned}$$

In the above rules the matrix A_1 is obtained from (13) in the following manner. First, values of x_{10}, x_{11}, and x_{15} are chosen such that $F_1^1(x_{15}) = 1$, and $F_2^1(x_{10}, x_{11}) = 1$, namely, these are $x_{10} = x_{11} = -\pi/4$, and $x_{15} = 5\pi/18$. Second, we replace the previous values in (13) where A_1 is given by the equations associated with $(\dot{x}_3, ...\dot{x}_{12})$. The matrix B is represented by the equations associated with $(\dot{x}_{13}, ...\dot{x}_{16})$, and is thus the same for all the rules. For illustration, we give the expression of the state-space representation for the first rule. If $x_{15} = 5\pi/18$ and $\cos x_{10}\cos x_{11} = 0.5$ then

$$A_1 = \begin{bmatrix} 0_4 & 1_4 & 0_4 \\ 0_4 & G_4 & H_4 \\ 0_4 & 0_4 & S_4 \end{bmatrix};\ B = \begin{bmatrix} 0_4 \\ 0_4 \\ -S_4 \end{bmatrix};$$

$$C = \begin{bmatrix} 1_4 & 0_4 & 0_4 \\ 0_4 & 1_4 & 0_4 \end{bmatrix};\ D = \begin{bmatrix} 0_4 \\ 0_4 \end{bmatrix}\ and\ a(\theta) = \begin{bmatrix} 0_4 \\ N \\ 0_4 \end{bmatrix}$$

where "0_i" is a zero matrix of rank i, "1_i" identity matrix of rank i, and G_4, S_4 and H_4 given by:

$$G_4 = \begin{bmatrix} 0 & 0 & g_3 & 0 \\ g_1 & 0 & 0 & 0 \\ 0 & g_2 & 0 & 0 \\ 0 & 0 & 0 & f \end{bmatrix}; \; S_4 = 300 \cdot 1_4$$

$$H_4 = \begin{bmatrix} 0 & 0 & 0 & 0 \\ 0 & -a & 0 & 0 \\ 0 & 0 & -b & 0 \\ 0 & 0 & 0 & -c \end{bmatrix}; \; and \; N = \begin{bmatrix} n_1 \\ n_2 \\ n_3 \\ n_4 \end{bmatrix}$$

In G_4, $g_1 = 0.8727dK_M\Omega_M^2$, $g_2 = -0.8727eK_M\Omega_M^2$, and $g_3 = -0.5K_M\Omega_M^2$; and in N, $n_1 = Z_w + Z_s$, $n_2 = N_\phi$, $n_3 = N_\theta$, and $n_4 = N\psi + f\psi_T$. The rest of A_2, A_3, and A_4 are obtained in the same manner. The global model resulting from the fuzzy rules corresponds to the one from the system described by (2), where the entries of C related to altitude/attitude angles and their rates are equal to 1, and furthermore C is identical for all rules ($C_i = C$). Also, $D_i = D = 0$. Thus the global TS- fuzzy model corresponding to (13) is given as:

$$\begin{aligned} \dot{x} &= \sum_{i=1}^{4} w_i(x_{10}, x_{11}, x_{15})(A_i x + Bu) + a(\theta) \\ y &= \sum_{i=1}^{4} w_i(x_{10}, x_{11}, x_{15})(C_i x) = Cx \end{aligned} \tag{18}$$

In the above, w_i is the degree to which a rule is activated given some values for x_{10}, x_{11}, and x_{15}. Their expressions are given as

$$\begin{aligned} w_1 &= F_1^1(x_{15}) \cdot F_2^1(x_{10}, x_{11}) \\ w_2 &= F_1^1(x_{15}) \cdot F_2^2(x_{10}, x_{11}) \\ w_3 &= F_1^2(x_{15}) \cdot F_2^1(x_{10}, x_{11}) \\ w_4 &= F_1^2(x_{15}) \cdot F_2^2(x_{10}, x_{11}) \\ and \quad & \sum_{i=1}^{4} w_i = 1 \end{aligned}$$

Given the TS-fuzzy model in (18), a FGS dynamic output feedback $\mathcal{H}_\infty$ controller can be designed as described in Section IV-A. In particular, using (4) and (10) the controller is then of the form:

$$\begin{bmatrix} \dot{x}_c \\ u \end{bmatrix} = \sum_{i=1}^{4} w_i \begin{bmatrix} A_c^i & B_c^i \\ C_c^i & D_c^i \end{bmatrix} \begin{bmatrix} x_c \\ y \end{bmatrix}, \tag{19}$$

The controller is designed so that it can track desired altitude and attitude angles. Integral action is introduced to avoid steady state errors in the altitude/attitude loop control. The control scheme is illustrated in Fig. 6. The integral action is a first-order integrator of time constant $\tau = 1s$ and it permits the synthesis of region-wise $\mathcal{H}_\infty$ controllers verifying the Lyapunov global stability conditions. $(x_{13}, ...x_{16})$ are in the range [-1, +1] and this is accounted for in the controller design. The servo state x_{15} must be measured because of its use in the scheduling.

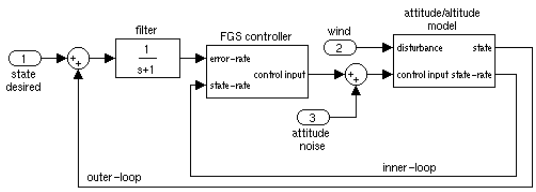

Fig. 6. Fuzzy gain scheduler for the attitude/altitude loop

VI. Simulation results

The purpose with this section on numerical experimentation is to demonstrate the following two features of the controller developed in the previous section:

- First, its robustness w.r.t. external disturbances such as wind, mass change, and sensor-noise on the attitude control signals.
- Second, the ability to perform stable aggressive flying defined by fast acceleration / deceleration, climb / descent, and sharp/smooth turns.

The experimental results reported here are derived in simulation using the nonlinear model described in Section V. The experiments on robustness solely relate to the robustness of the attitude/altitude loop control. The reason for this is as follows: the control of VTOL is done by changing the attitude angles for a desired altitude. The experiments on "aggressive" flight relate to the attitude/altitude controllers. Experimental results on curvilinear trajectory tracking at high speed are reported in [16].

A. Robustness

To illustrate robustness we consider in this section

- the FGS attitude controller where the control input s$(b_{1s}, a_{1s}, \theta_T)$ to the attitude angles are subject to noise.
- the FGS altitude controller subject to external disturbances in terms of mass change and wind change.

1) Attitude control robustness: The numerical experiments are performed with the FGS controller from Section IV, i.e., the attitude/altitude loop FGS controller.

Experiment 1: The task to perform consists in regulating the attitude angles w.r.t certain desired values (set-point control), given that the control inputs for the attitude angles are affected by white noise. The experiment is performed with a constant mass of 50 Kg and a constant wind speed of 10 m/s. A noise with a high frequency is introduced to the model. This noise can be induced by vibrations on the control inputs and overload the servo-actuators. In the simulation we use a white-noise to simulate its effect. The attitude control noise model takes as input a white-noise $N_n(0, 2)$ which is is a stochastic process defined by an amplitude $\approx 5 - 10\%$ of the control inputs, a mean-value 0, and a variance of 2. We introduce the 3rd-order filter of equation (20) in order to cancel the noise effect on the attitude angles' control inputs.

$$H(s) = \frac{248.05}{s^3 + 125.66s^2 + 7895.68s + 50} \tag{20}$$

In the context of this experiment (see Fig. 7), we compare the

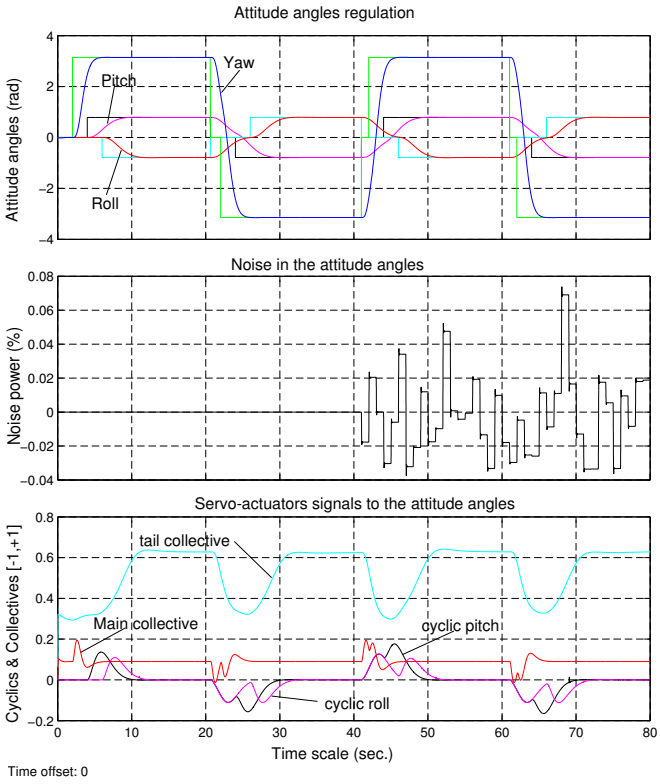

Fig. 7. Exp.1: Attitude angles set-point regulation (up), with and without added noise (middle), and related actuators outputs profiles for altitude and attitude (bottom).

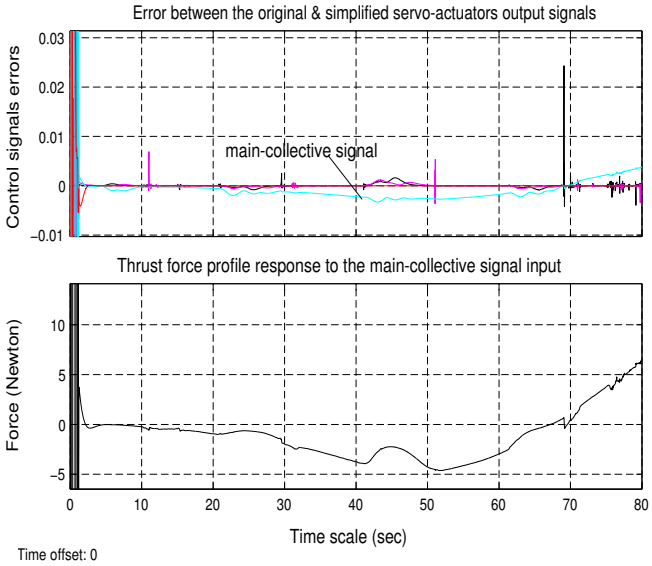

Fig. 8. Exp.1: Error between original & simplified servo-actuators output signals (top), and main-rotor force profile (bottom)

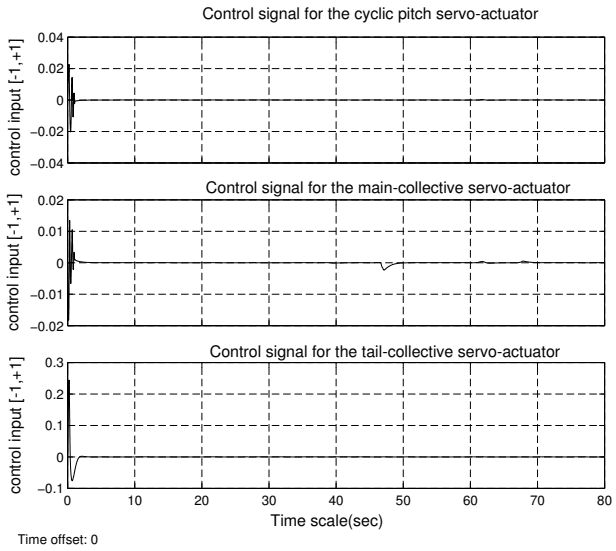

Fig. 9. Exp.1: Control input signals to the actuators, for roll (top), pitch (middle), and yaw (bottom).

controller performance with and without noise on the control inputs for the attitude angles. The upper-part of the figure illustrates the attitude angles. These are subject to set-point control at their extreme values ($[\phi;\theta;\psi] = [\pm\frac{\pi}{4};\pm\frac{\pi}{4};\pm\pi]$). The middle-part shows the injection of $\approx 5-10\%$ white noise to the attitude control signals after a 80 seconds of simulation. The bottom-part of the figure illustrates the magnitude of the control inputs to the attitude angles from the actuators. As one can see, this does not affect the controller inputs nor the attitude angles profiles. The settling time for the pitch and the roll is 6 seconds, and 3 seconds for the yaw. We should be able to perform the attitude control within the above-specified ranges without saturating the servo-actuators. Fig. 8 upper-part shows a comparison between the outputs from simplified and original servo-actuators. The lower-part of the figure illustrates the impact of the outputs from the servo-actuators on the thrust force: a slight drift of the collective pitch has a direct influence on the trust force of $\pm 5N$. The need for the results presented in Fig. 8 is as follows: The output of the servo-actuators causes a change in the main rotor force. So it is necessary to verify that the simplifications made both at the level of the servo-actuators and at the attitude dynamics levels approximate as close as possible their original counterparts. From Fig. 9, we can verify that this is indeed the case. It shows that the attitude angles are affected by neither the approximation made on the actuators model nor the introduction of noise to the attitude control inputs. The control signals to the attitude angles do not exceed the limits, imposed by the servo-actuators of the original model ($[-1,+1]$).

Experiment 2: The task to perform consists in tracking desired trajectories for the attitude angles, given that the control inputs to these angles are affected with noise. The experiment is performed with a constant mass of the helicopter of 50 Kg and a constant wind speed of 10 m/s.

Fig. 10 top-part shows the tracking errors for the roll, pitch, and yaw angles. The attitude trajectories tracked are of sinusoidal shapes. The simulation is executed without noise first, then, after 80 seconds a noise of 5 to 10 % of the amplitude of the control inputs is introduced (see middle-part). The bottom-part of the figure illustrates the actuated signals resulting from the control inputs to the attitude angles: The oscillatory signals represents the actuated attitude inputs (tail-

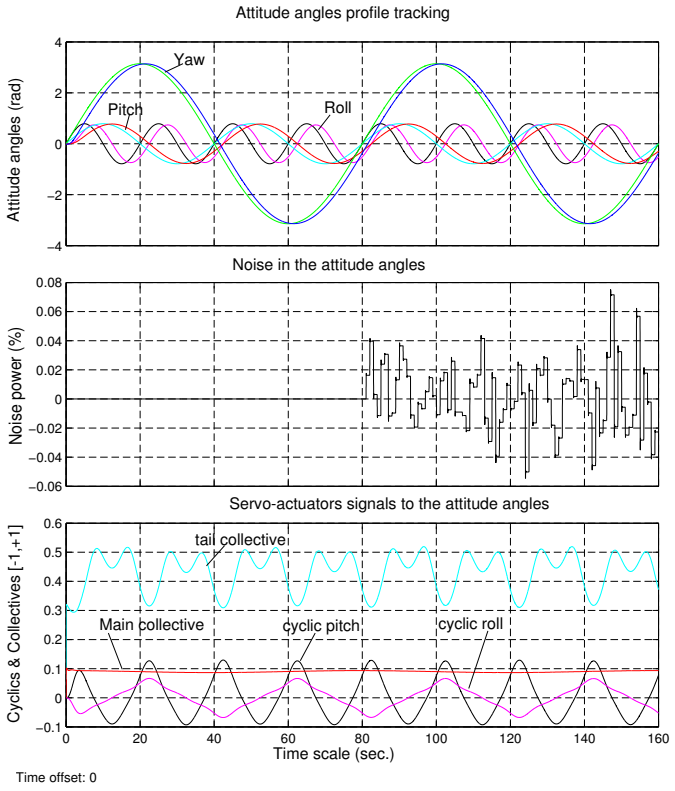

Fig. 10. Exp.2: Attitude angles tracking (up), with and without added noise (middle), and related actuators outputs profiles for altitude and attitude (bottom).

collective and cyclic angles), and the constant signal is the one responsible for maintaining the altitude to a desired value (main-collective). As the figure clearly shows, the noise affects neither the servo-actuator signals nor the attitude angles' responses. The settling time is approximately 3 seconds for the pitch and roll angles, and about 2 seconds for the yaw. Fig. 11 bottom-part shows the main rotor force profile. The main rotor force amplitude does not in this case exceed a range of $\pm 4N$, which is the equivalent of a fluctuation of the body mass of ≈ 0.4 Kg. The upper-part of the figure shows the error between signals generated from the original and the simplified servo-actuator models. One can see that it is mainly the main-collective signal that has an influence on the main rotor force. Fig. 12 shows that as in Exp.1, the attitude angles are affected by neither the noise nor the approximation made on the actuators. The attitude angles do not exceed the limits, imposed by the servo-actuators original model ($[-1, +1]$). Thus the simplified servo-actuators' model –represented as 1st-order transfer function– with time constant $\tau = 20ms$ and a saturation bounds [-1,+1] approximates well enough the original servo-actuators' model.

2) Wind and mass effects on altitude control:

Experiment 3: The task in this experiment consists in tracking an altitude trajectory taking into account the accumulated effect of wind variations and body mass changes.

The wind model used in the simulator takes as input a three dimensional wind speed V_W, and is described by the following

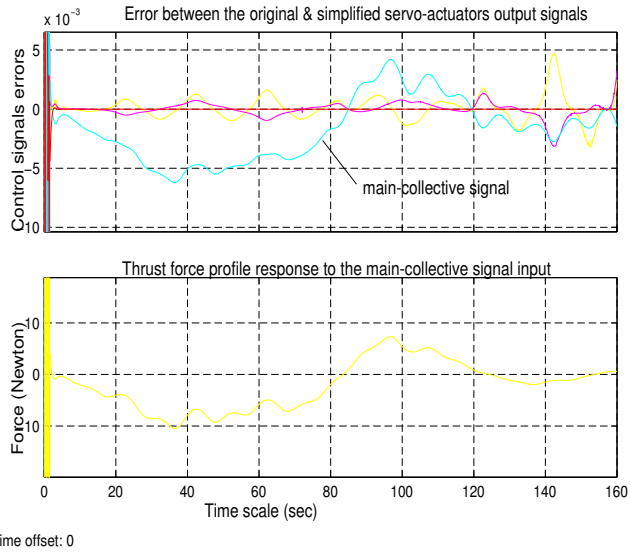

Fig. 11. Exp.2: Error between original & simplified servo-actuators output signals (top), and main-rotor force profile (bottom)

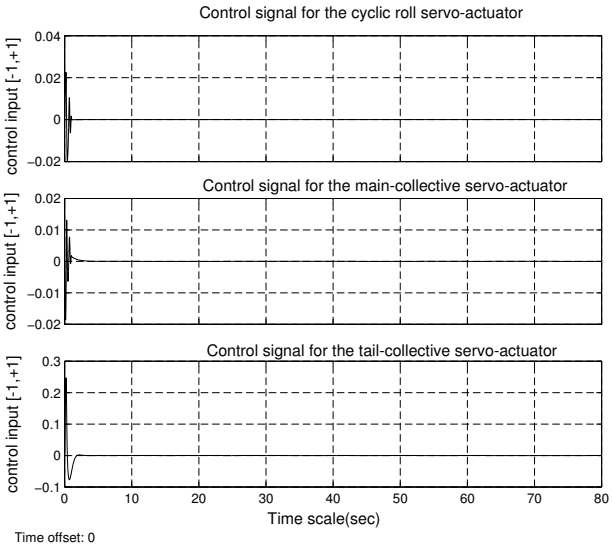

Fig. 12. Exp.2: Control input signals to the actuators, for roll(up), pitch (middle), and yaw (bottom).

expression

$$\vec{\mathcal{F}}_W = N_w(0,2) + \frac{1}{2} C_d A_C V_W^2; \qquad \text{with} \qquad (A_C = 4\pi R_C^2)$$

where $N_w(0,2)$ is a stochastic process defined by a white noise of amplitude $1m/s^{-2}$, a mean-value 0, and a variance of 2, and represents the wind turbulence (i.e. gusts). $\frac{1}{2} C_d A V_W^2$ is the cabin reaction to its motion and wind force (i.e. cabin drag force). A_C is the area of the cabin in each direction, and C_d is a given drag coefficient. Fig. 13 illustrates the block model for the wind, utilized in the simulation. The output of this model block is connected to input-2 of the block-model shown in Fig. 6. Fig. 14 upper-part illustrates the wind turbulence profile after filtering. The middle-part shows the cabin drag-force profile. The bottom-part of the figure shows a

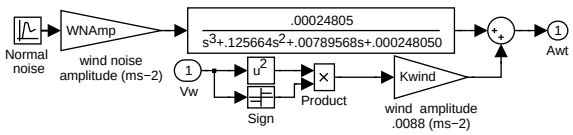

Fig. 13. The wind turbulence and drag-force components model

diagram representing the resulting sum of wind turbulence and cabin drag-force. We may conclude from these profiles that the turbulence involved in this process is negligible w.r.t the cabin-drag force. A mass change has an effect on the acceleration

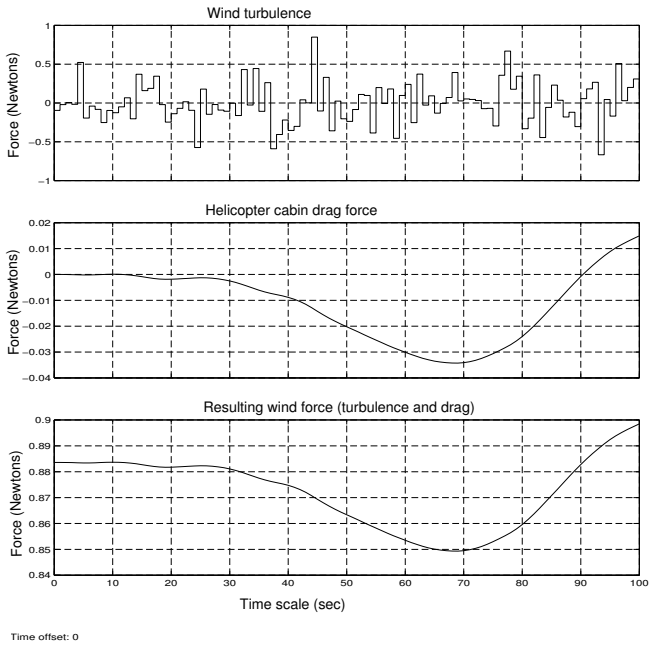

Fig. 14. Wind turbulence (up), drag-force (middle), and total wind force profiles (bottom) [Newtons]

of the solid body. In the VTOL case, the force provided by its rotor counteract the effect of gravity by its lift component. The total force of the rotor has to be big enough to : 1) afford the lift necessary to maintain the heave of the helicopter; and/or 2) perform ascend motion, and/or 3) produce a thrust for horizontal motion enough large to counteract the drag due to wind action on the body. The mass of the helicopter may change for different reasons. One is that the helicopter is loaded with a sensory platform, which is equivalent to a mass increase from 0 to 20 Kg. The other reason is the gas volume decrease during the flight, which varies the mass of the helicopter from 50 Kg (without payload) to 45 Kg –for a fuel reservoir of 5 liters and a fuel consumption assumed constant along time. Fig. 15 top-part shows the tracking of a sinusoidal altitude profile, given a varying wind speed illustrated by the figure's bottom-part, and a decreasing mass as shown in the 3rd diagram from top. Second diagram from top illustrates the control inputs (collective's and cyclic's) needed to achieve the altitude profile tracking. The diagrams show clearly that a variation in the wind force in any direction up to a reasonable

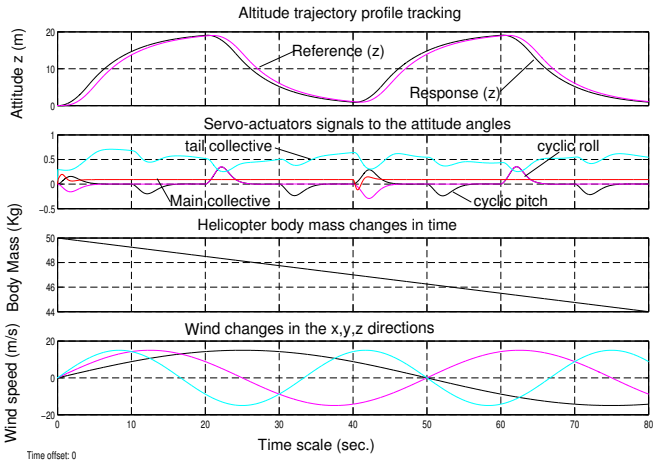

Fig. 15. Exp.3: Altitude-tracking [meters] (up), and control signals (2nd from top), w.r.t body mass change [Kg] (3rd from top), and wind fluctuation [m/s] (bottom).

magnitude, and a decrease of the the VTOL mass do not affect the control inputs values, and thus do not affect the good tracking of the desired altitude profile.

3) Limitation on the altitude controller: There are two limitations imposed on the action of the altitude controller.

1) a limit on the control output that is, all of the control signals producing the cyclic's (pitch and roll), and collective's (main and tail) are in the interval $[-1, +1]$. This is due to limitations on the signals affordable by the servo-actuators.
2) a limit w.r.t the magnitude of change in reference value for the altitude. It turns out that a new reference value can be set max 10 meters away from the previous one.

To cope with the second limitation, we adopt a simple 1st-order integrator with saturation. It is similar to the one used for the servo-actuator, but with a time constant $\tau = 20ms$ and a first-order filter with time constant $\tau = 9sec$. The integrator shapes the altitude reference value from step to ramp, and in this way, allows for a change of reference values for up to 300 meters. This is achieved still with the control inputs (cyclic's and collective's) being within the range of $[-1, +1]$. It has to be noted here that all the following experiments are performed with the original model using the controller derived on the basis of the simplified model.

B. Aggressive flying

To illustrate aggressive flying only based on the use of the attitude controller we consider:

- set-point velocity control for the purpose of fast acceleration/deceleration,
- set-point and tracking control for heading, with the purpose of performing turns and curvilinear motion patterns.

1) Fast acceleration/deceleration:

Experiment 4: The task consists in accelerating/decelerating by set-point control of reference velocities while keeping a constant heading ($\chi = 0$).

The experiment is performed with body mass of 50 Kg and a wind speed of 10 m/s. One can see the behavior of the x- and y-velocity channels when the reference speed change from $V = 0m/s$ to $15m/s$, i.e., the case of acceleration. From this velocity reference ($V(t) = 15m/s$), the helicopter should switch to $V(t) = 5m/s$, i.e., we have the case of deceleration. The reference velocities for longitudinal (x - channel) and lateral (y-channel) motion are translated (see [16]) into desired profiles for pitch and roll respectively. Thus, the attitude controller should execute these profiles in order to achieve the above mentioned velocities. The desired heading is translated (see [16]) into a desired profile for the yaw, and the attitude controller should execute this profile. Fig.

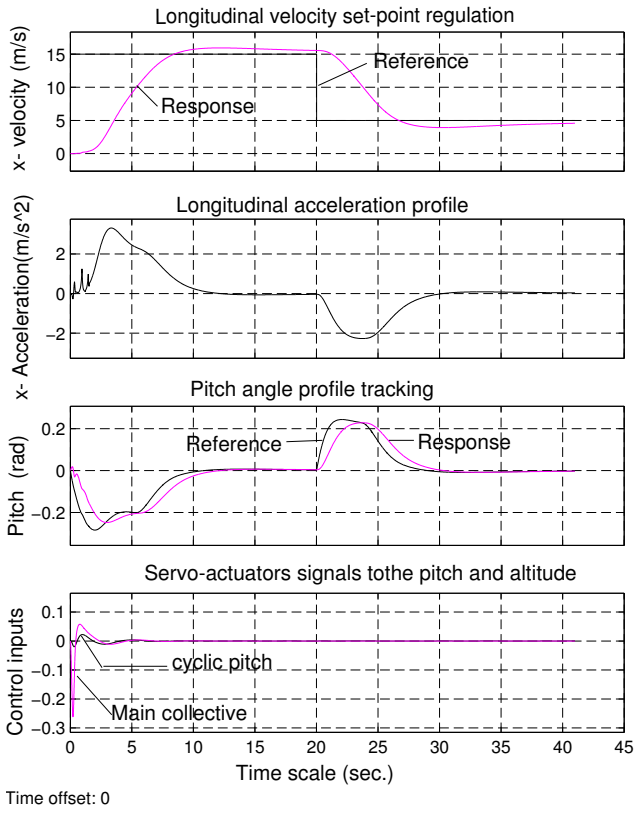

Fig. 16. Exp.4: Longitudinal velocity set-point regulation. Top to bottom: speed [m/s], acceleration $[m/s^2]$, angles [rad], and control signals.

16 illustrates the x-velocity channel. The upper-part of the figure presents the longitudinal velocity regulation as a result of changes of velocity reference set-points, while keeping the heading steady ($\chi = 0$). In the second diagram, we have the corresponding longitudinal acceleration. The third diagram in the figure illustrates the behavior of the pitch response needed to maintain the longitudinal speed to the desired set-point values. The bottom part of the figure shows the behavior of the control signals responsible to maintain the attitude coherent with the desired velocity. If the time-settlement for the pitch is $\approx 3seconds$, the time-rise to settle the velocity to its reference value might increase to 20 seconds. Fig. 17 illustrates the y-velocity channel. The upper-part of the figure presents the lateral velocity regulation as a result of

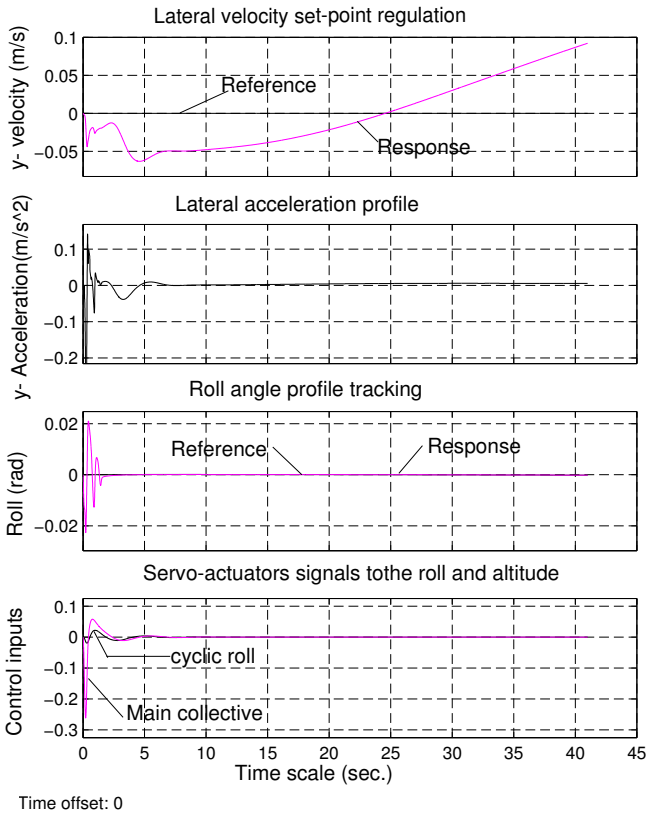

Fig. 17. Exp.4: Lateral velocity set-point regulation. Top to bottom: speed [m/s], acceleration $[m/s^2]$, angles [rad], and control signals.

change of velocity reference while keeping the heading steady ($\chi = 0$). In the second diagram, we have the corresponding lateral acceleration. The third diagram in the figure illustrates the behavior of the roll needed to maintain the lateral speed constant to zero, as we intended to accelerate only in the longitudinal direction. The bottom part of the figure shows the behavior of the control signals responsible to maintain the attitude coherent with the desired velocity.

2) Turns via heading control: In the following experiments, we will illustrate two types of turns: 1) a sharp turn is defined as a change of the reference value for heading, 2) a smooth turn is defined as the tracking of a given heading trajectory. The angle of a turn (ψ) or the yaw, is a function of the heading (χ). Thus the attitude controller should regulate/track a desired profile for the yaw which is obtained on the basis of the desired heading. The experiments are performed with a body mass of 50 Kg and a wind speed of 10 m/s.

Experiment 5: The task here will consist in performing some sharp turns by changing the reference heading while keeping constant the velocity ($V(t) = 17m/s$). The reference heading should take successively the following reference values ($\chi(t) = 0, \pi/2, \pi, 3\pi/2$) where each of these reference values is kept for ($t = 20seconds$).

Fig. 18 illustrates Exp.5. The upper-part shows changes in reference set-points for the heading and heading regulation response. In the bottom part we can see the resulting turns in terms of yaw angles, w.r.t the computed set-point profile for

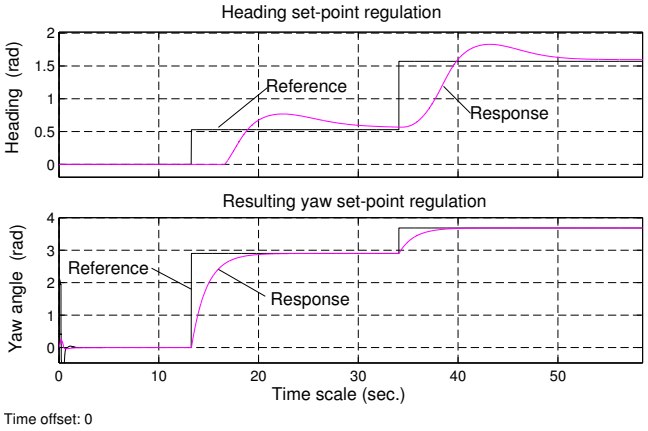

Fig. 18. Exp.5: Sharp turn profiles for the roll and pitch angles [rad]

the yaw related to the above changes in heading. The settling time for the yaw angle is about 3 seconds.

Experiment 6: The task consists in performing some smooth turns by tracking a reference heading trajectory while keeping constant the velocity ($V(t) = 15m/s$). The reference heading trajectory is given simply as ($\chi(t) = t/10, \chi \in [0, 2\pi[$ mod π).

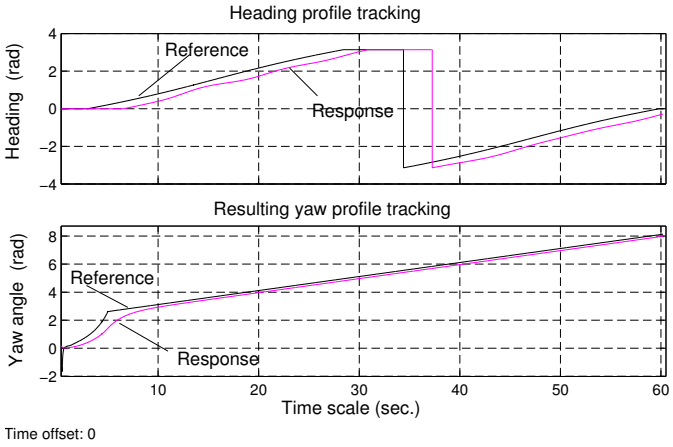

Fig. 19. Exp.6: Smooth turns for the roll and pitch angles [rad]

Fig. 19 illustrates Exp.6. The upper-part illustrates changes in reference profile and the heading tracking response to this profile. The bottom-part shows the smooth turns in terms of yaw profile, corresponding to the yaw references computed from the heading reference trajectory. The settling time for the yaw angle is about 3 seconds.

3) Curvilinear motion patterns at high speed: Executing curvilinear motion patterns can be done in two ways: 1) specifying a desired pattern in terms of Cartesian coordinates, 2) using heading, yaw and speed control. In the first case, one would need a position controller. In this work we will resort to the second option, where the desired curvilinear motion pattern or trajectory is defined in terms of desired velocity magnitude V^d, and its orientation χ^d. These in turn are transformed into desired profiles for attitude angles at a given altitude and these desired profiles are achieved by the attitude controller. Another issue here is the way in which the helicopter flies along a desired pattern or curvilinear trajectory, defined in the above terms. Let ψ^d or yaw be the angle between the nose of the helicopter and the x-axis of the inertial frame. Given a desired trajectory in the body frame, the desired value ψ^d is a function of $\dot{x}$ and $\dot{y}$ transformed from the body to the inertial frame. Thus

1) flying nose-on-the-trajectory means tracking of ψ^d.
2) flying nose-off-the-trajectory means that we maintain the yaw angle ψ^d constant.

In the next experiments, we will perform nose-on-the-trajectory type of flights.

Experiment 7: The task consists in following a predefined rectangular motion pattern. This pattern is defined by successive changes of desired heading $\chi(t) = 0, \pi/2, \pi, 3\pi/2$. The desired magnitude of the velocity is $V(t) = 17m/s$ where each of these reference values is kept for ($t = 25seconds$).

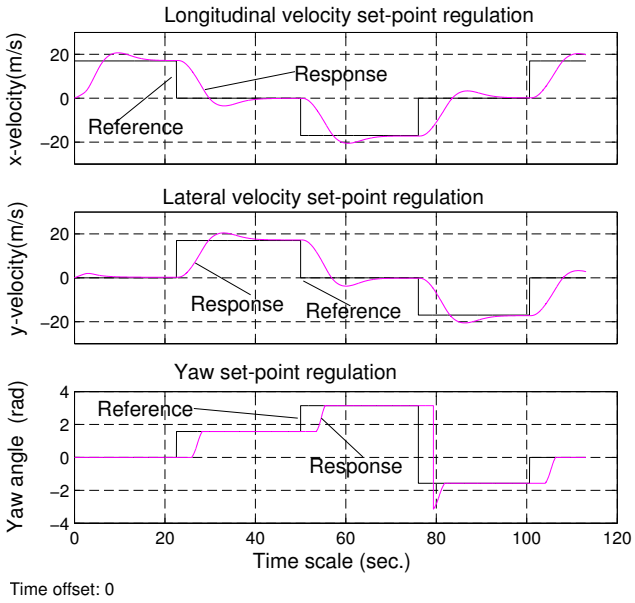

Fig. 20. Exp.7: Rectangular pattern path to be followed by the helicopter: Velocity set-point profiles for the x, y, and yaw channels.

Fig. 20 top-part shows the responses in velocity profiles to achieve in order to do fly along a rectangular pattern. In the upper-part of the figure, we see the response of the $\dot{x}$-channel to changes of set-points in translational speeds. The middle-part of the figure illustrates the regulation of the lateral velocity w.r.t changes in reference set-points for the $\dot{y}$-channel. The bottom-part of the figure illustrates the yaw profile set-point regulation to achieve the desired rectangular pattern motion. Fig. 21 shows the log of position translations along a rectangular pattern as a result of the changes in set-points of the yaw and a constant velocity.

Experiment 8: The task here consists in following a predefined circular motion pattern. This pattern is defined by desired heading trajectory $\chi(t) = t/10, \chi \in [0, 2\pi]$ modulo π. The desired magnitude of the velocity is $V(t) = 17m/s$.

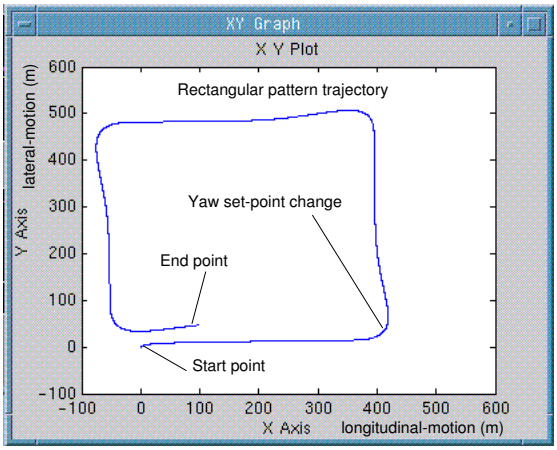

Fig. 21. Exp.7: Rectangular pattern path to be followed by the helicopter: Trajectory log of positions (x,y)

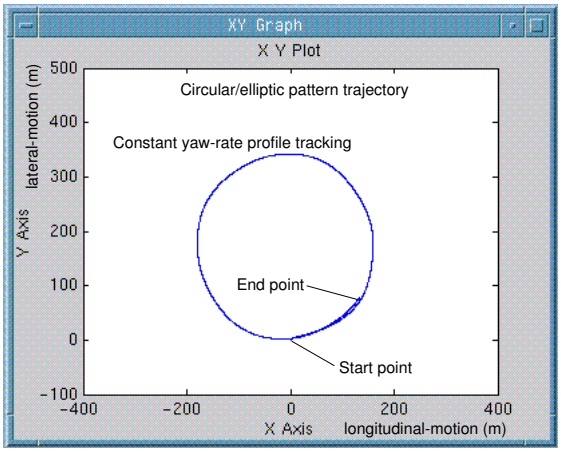

Fig. 23. Exp.8: Circular pattern path to be followed by the helicopter: Trajectory log of positions (x,y)

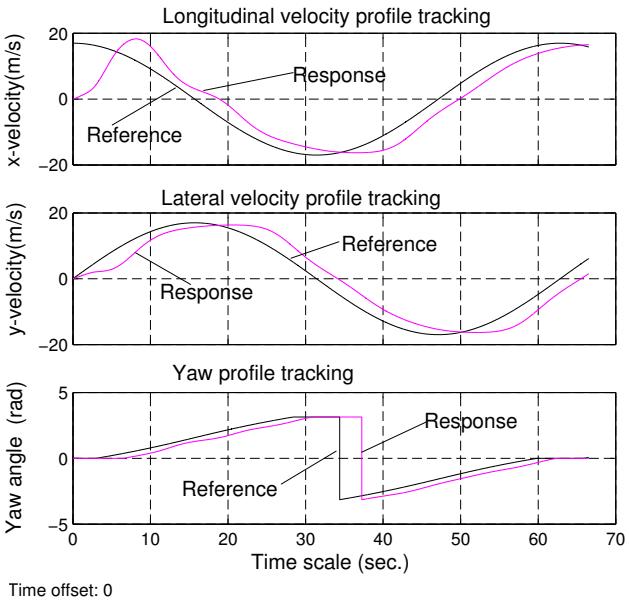

Fig. 22. Exp.8: Circular pattern path to be followed by the helicopter: Velocity profiles tracking for the x, y, and yaw channels.

Fig. 22 top-part shows the responses in velocity profiles to achieve in order to do fly along a circular pattern. In the top-part of the figure, we see the response of the $\dot{x}$-channel to a profile of translational speeds to track. The middle-part of the figure illustrates the tracking of the lateral velocity w.r.t a profile for the $\dot{y}$-channel. The bottom-part of the figure illustrates the yaw profile tracking to achieve the desired circular pattern motion. Fig. 23 shows the log of position translations along a circular pattern as a result of a constant value of the yaw rate and a constant velocity.

VII. Conclusions

This paper presented a novel method for the design of a fuzzy gain scheduled attitude/altitude controller for the unmanned APID-MK3 helicopter. The controller is based on a realistic nonlinear MIMO model of the actual helicopter platform. It has been has been tested in extensive simulation, showing its stability and robustness with respect to external disturbances in terms of wind and gusts, and perturbations induced by the rotors vibrations. The results show the effectiveness of the proposed design method: The ability of the control to perform aggressive flying has been approached from the prospect of acceleration/deceleration and attitude angles maneuvers. Both permitted to illustrate the possibility of performing particular geometrically-shaped trajectories.

Acknowledgment

The authors would like to express their gratitude to the Knut and Alice Wallenberg Foundation in Sweden whose financial support made this work possible. They would like to thank the anonymous reviewers for their comments that helped to improve the quality of this paper.

References

[1] T. Takagi, and M. Sugeno, *Fuzzy identification of Systems and its Applications to Modeling and Control*, In: IEEE Trans. Systems, Man and Cybernetics, SMC-15(1), pp. 116–132, Jan. 1985.

[2] T.J. Koo et al., *Hierarchical Hybrid System Design on Berkley UAV*, In: Int. Aerial Robotics Competition, Richland, WA-USA, Aug. 1998.

[3] E. Frazzoli, et al., *A Hybrid Control Architecture for Aggressive Manoeuvring of Autonomous Helicopters*, In: Proc. 38th Conf. on Decision and Control, Phoenix, AZ-USA, Dec. 1999.

[4] H. Shim, T.J. Koo, F. Hoffmann, and S. Sastry, *A Comprehensive Study of Control Design for an Autonomous Helicopter*, In: Proc. 37th IEEE Conf. on Decision and Control (CDC'98), pp. –, Tampa, FL-USA, Dec. 1998.

[5] T. J. Koo, and S. Sastry, *Output tracking control design of a helicopter model based on approximate linearization*, In: Proc. 37th IEEE Conf. on Decision and Control (CDC'98), pp. 3635–3640, Tampa, FL-USA, Dec. 1998

[6] P. Bendotti, and J.C. Morris, Identification and Stabilization of a Model Helicopter in Hover, In: American Control Conf. (ACC'95), Seattle, WA-USA, 1995.

[7] J.V.R. Prasad, A.J. Calis,e Y. Pei, and J.E. Corban, *Adaptive Non-linear Synthesis and Flight Test Evaluation on an Unmanned Helicopter*, In: 1999 IEEE Int. Conf. on Control Applications (ICRA'99), Antwerp, Belgium, 1999.

[8] J.E. Hanser, *Approximate Tracking for Nonlinear Systems with Application to Flight Control*, PhD thesis, College of England, University of California, Berkeley, CA-USA 1989.

[9] P. Bergsten, *Observers and Controllers for Takagi-Sugeno Systems* PhD thesis Orebro Studies in technology 1, Orebro, Sweden, 2001.

[10] M. Sugeno, Development of an intelligent Unmanned Helicopter, In: *Fuzzy Modeling and Control, Selected works of M. Sugeno*, T. H. Nguyen and N. R. Prasad (Eds.), CRC Press, pp. 13–43, Boca Raton, FL-USA, 1999.
[11] G. J. Klir, and B. Yuan, *Fuzzy Sets and Fuzzy Logic: Theory and Applications*, Prentice Hall, New Jersey, USA, 1995.
[12] P. Korba, *A Gain-Scheduling Approach to Model-Based Fuzzy Control*, VDI Verlag GmbH, 837, Fortschritt-Berichte VDI, Reihe 8 Meß-, Steurungs- und Regelungstechnik Series, Düsseldorf, Germany, 2000.
[13] K. Tanaka et al., *Generalized Takagi-Sugeno Fuzzy Systems: Rule Reduction and Robust Control*, In: 9th IEEE Int. Conf. on Fuzzy Systems, 2: pp. 688–693, San Antonio, TX-USA, May 2000.
[14] S. Boyd et al., *Linear Matrix Inequalities In System and Control Theory*, Studies in Applied Mathematics Series, SIAM, Philadelphia, USA, 1994.
[15] O. Amidi, T. Kanade, and J.R. Miller, *Autonomous Helicopter Research at Carnegie Mellon Robotics Institute*, In: Proceedings of Heli Japan '98, Apr. 1998.
[16] B. Kadmiry, D. Driankov, *A fuzzy flight controller Combining Linguistic and Model-Based Fuzzy control*, to appear in International Journal of Fuzzy Sets and Systems (FSS), Elsevier, to be published.

Bourhane Kadmiry Bourhane Kadmiry received the BSc degree in Applied Math. & Computer Sc., the MSc degree in Applied Math. & Computer Sc., the MSc degree in Control Theory & Computer Engineering, and the MSc degree in Instrumentation & Measurement from the University of Rouen, Faculty of Sciences, Rouen, France; and the Licentiate degree in Computer Engineering from the Univ. of Linköping, Linköping, Sweden in 1993, 1994, 1995, and 2002 respectively. From 1998 he was with the Division for Artificial Intelligence and Integrated Computer Systems (WITAS), Dept. of C.Sc., Univ. of Linköping. He is completing his PhD current 2004, and his current research interests and activities are in the areas of fuzzy control, and perception-based control for autonomous aerial vehicles.

Dimiter Driankov Dimiter Driankov received the BSc Math. degree, the MSc degree in Computer Sc. from the University of Sofia, Faculty of Mathematics, Sofia, Bulgaria, and the PhD degree in Computer Sc. from the Univ. of Linköping, Linköping, Sweden in 1973, 1975, and 1988 respectively. From 1985 to 2000 he was with the Dept. of Comp. Sci., Univ. of Linköping where he was heading the Autonomous Systems Lab (1996-1999). He was also a visiting professor with the Division for Artificial Intelligence and Integrated Computer Systems (WITAS) at this department and a member of the Wallenberg Lab for Information Technology and Autonomous Systems (2000-2003). Since 2001 he is a professor at the Technology Dept., Örebro Univ., Örebro, Sweden and is now a research director for the Applied Autonomous Sensor Systems Center. He has co-authored and authored more than 40 conference, journal articles, and book chapters, 2 books, and 3 edited volumes in the areas of fuzzy logic and fuzzy control. He is a coordinator for a EC Marie Curie Training Site in the area of autonomous robotic systems. His current research interests and activities are in the areas of model-based fuzzy control, computational theories of perception, and perception-based control of autonomous vehicles.